Accepted Manuscript

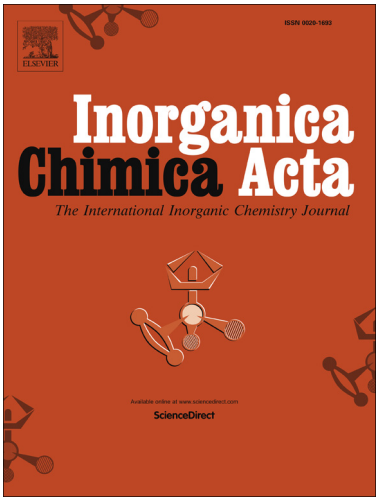

Mixed-Valence μ_3-Oxo-Centered Triruthenium Cluster $[Ru_3{}^{(II,III,III)}(\mu_3\text{-}O)(\mu\text{-}CH_3CO_2)_6(H_2O)_3]\cdot 2H_2O$: Synthesis, Structural Characterization, Valence-State Delocalization and Catalytic Behavior

Alla Dikhtiarenko, Sergei Khainakov, José R. García, José Gimeno

PII: S0020-1693(16)30288-2
DOI: http://dx.doi.org/10.1016/j.ica.2016.05.046
Reference: ICA 17082

To appear in: *Inorganica Chimica Acta*

Received Date: 18 January 2016
Revised Date: 18 May 2016
Accepted Date: 19 May 2016

Please cite this article as: A. Dikhtiarenko, S. Khainakov, J.R. García, J. Gimeno, Mixed-Valence μ_3-Oxo-Centered Triruthenium Cluster $[Ru_3{}^{(II,III,III)}(\mu_3\text{-}O)(\mu\text{-}CH_3CO_2)_6(H_2O)_3]\cdot 2H_2O$: Synthesis, Structural Characterization, Valence-State Delocalization and Catalytic Behavior, *Inorganica Chimica Acta* (2016), doi: http://dx.doi.org/10.1016/j.ica.2016.05.046

Mixed-Valence μ_3-Oxo-Centered Triruthenium Cluster $[Ru_3^{(II,III,III)}(\mu_3\text{-}O)(\mu\text{-}CH_3CO_2)_6(H_2O)_3]\cdot 2H_2O$: Synthesis, Structural Characterization, Valence-State Delocalization and Catalytic Behavior

Alla Dikhtiarenko, Sergei Khainakov, José R. García and José Gimeno

Departamento de Química Orgánica e Inorgánica, Universidad de Oviedo – CINN, 33006 Oviedo, Spain

Abstract

The oxo-centered, trinuclear, mixed valence $[Ru_3^{(II,III,III)}O(CH_3CO_2)_6(H_2O)_3]\cdot 2H_2O$ (**2**) acetate complex has been prepared with high yield through reduction of $[Ru_3^{(III,III,III)}O(CH_3CO_2)_6(CH_3OH)_3]\cdot CH_3CO_2$ precursor compound in presence of muccic acid under hydrothermal conditions. The crystalline trinuclear oxo-cluster has been obtained as crystalline powder and characterized by single-crystal and powder X-ray diffraction, elemental analysis, SEM, TGA, IR spectroscopy. Complex **2** composes of μ_3-oxocentered trinuclear ruthenium array and exhibits the oxidation state delocalization between three Ru atoms at 293 K. Accurate single-crystal analysis along with valence bond calculations reveal trapped-valence state delocalization at room temperature, whereas three-site relaxation occurs at 100 K leading to Ru(II) and Ru_2(III) formal states. Moreover, the mixed valence of $Ru^{II}Ru_2^{III}$ unit in compound **2** has been confirmed by XANES spectroscopy. The catalytic behavior of oxo-centered triruthenium complex **2** has been examined in hydration of nitriles and isomerization of allylic alcohols reactions both realized in aqueous media.

Keywords: Triruthenium oxo-cluster, mixed-valence delocalization, synthesis, hydration of nitriles, isomerization of allylic alcohols, catalysis.

1. Introduction

Triangular μ-oxo-centered ruthenium-carboxylate clusters of general formula $[Ru_3O(RCO_2)_6L_3]^n$ (R = H, CH_3, C_2H_5, C_3H_7, C_3F_7, C_6H_5, C_7H_{15}, C_8H_{16}; L = H_2O, PPh_3, CO, CH_3OH, *N*-heterocycles, $OS(CH_3)_2$, etc.) [1-10], where three ruthenium atoms are bridged by the oxygen atom located at the center of a ruthenium triangle and also by the six carboxylate ligands in the circumference (Scheme 1), show multiple redox behavior, intriguing mixed-valence chemistry, and versatile catalytic properties [11-14].

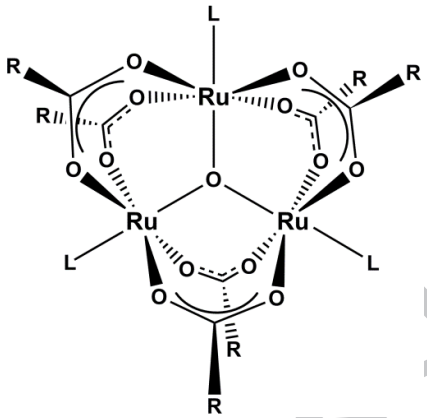

Scheme 1. (*single column fitting image*) Molecular structure of basic oxo-centered ruthenium carboxylate complex.

The axial ligands L are comparatively labile and can readily be substituted, thus enhancing significantly the richness of triruthenium chemistry. Moreover, along axial ligand substitution, the bridging carboxylates of oxo-centered triruthenium core $[Ru_3(\mu_3\text{-}O)(\mu\text{-}RCO_2)_6]^n$ can be replaced affording an excellent means to control the chemical and electronic properties by introducing proper organic ligands [15-17]. Nowadays, metal-oxo clusters gained particular interest as class of compounds that can be used as predesigned building blocks to elaborate functional hybrid materials such as metal-organic frameworks (MOFs) [17-21]. Among the variety of $[Ru_3O(RCO_2)_6L_3]^n$ clusters, considerable attention has been paid to those that has a mixed-valence state of ruthenium atoms, e.g. $[Ru_3^{II,III,III}O(RCO_2)_6L_3]^0$, because their original spectral and catalytic behavior [11, 22, 23]. The synthetic methodology for preparation of $[Ru_3^{II,III,III}O(RCO_2)_6L_2L']$ complexes (L = L´ = H_2O, pyridine; L´ = CO) involves the reduction of $[Ru_3^{(III,III,III)}O(CH_3CO_2)_6(CH_3OH)_3]^+$ cationic derivatives [6, 7, 9]. Nevertheless, the reduction process for the synthesis of the aqua-complex $[Ru_3^{II,III,III}O(CH_3CO_2)_6(H_2O)_3]^0$ implies rigorous conditions since a stream of hydrogen at 2 atm pressure through an aqueous solution and in presence of platinum oxide catalyst is required. In addition to the high cost of the method, the oxo-centered triruthenium (II,III,III) cluster core frequently undergoes a second step reduction step leading to binuclear μ-tetraacetate $Ru^{II}Ru^{III}$ product with loss of the central μ-oxo ion [7, 24].

Herein, we report the direct synthesis of $[Ru_3^{(II,III,III)}O(CH_3CO_2)_6(H_2O)_3]\cdot 2H_2O$ (**2**) straining from $[Ru_3^{(III,III,III)}O(CH_3CO_2)_6(CH_3OH)_3]\cdot CH_3CO_2$ (**1**) precursor complex under hydrothermal conditions which has been isolated as a crystalline powder in high yield using muccic acid as a one electron mild reduction agent. The structural characterization of $[Ru_3^{(II,III,III)}O(CH_3CO_2)_6(H_2O)_3]\cdot 2H_2O$ in solid state by X-ray diffraction is also described. In addition, mixed-valence delocalization in the $[Ru_3^{(II,III,III)}O(CH_3CO_2)_6(H_2O)_3]$ complex at room

temperature along with the catalytic activity in the hydration of nitriles and the isomerization of allylic alcohols in aqueous media, is discussed in details here.

2. *Experimental Section*

2.1. *Materials*

The compound $[Ru_3^{(III,III,III)}O(CH_3CO_2)_6(CH_3OH)_3]\cdot CH_3CO_2$ (**1**) was used as starting material for the preparation of **2** and was obtained by modifying the synthesis method reported by Spencer and Wilkinson [7]. Muccic acid and other chemicals are commercially available and were used as purchased.

2.2. *Synthesis of $[Ru_3^{(III,III,III)}O(CH_3CO_2)_6(CH_3OH)_3]\cdot CH_3CO_2$ (**1**)*

Following the modified procedure described by Baumann *et al*. [3], 3.0 g (12 mmol) of $RuCl_3\cdot 3H_2O$ and 6.0 g (44 mmol) of sodium acetate were dissolved in mixture of 75 mL of ethanol and 75 mL of glacial acetic acid. After being heated at reflux for 4 h or more, the solution was cooled. In order to separate the product from excess of non-reacted impurities, resulted solution was centrifuged for about 20 min at a medium speed and filtered. The resulting filtrate was reduced to green oil by removing the volatiles on a rotary evaporator. A total of 150 mL of CH_3OH was added to the oil substance, stirred and then filtered. The filtrate was cooled at - 40 °C for 4 h, and the precipitate of sodium chloride and sodium acetate was removed by filtration. Again, the resulting filtrate was evaporated on rotary evaporator, dissolved in methanol, filtered and evaporated. The pure acetate **1** was obtained by two recrystallizations from methanol-acetone, and subsequently dried in vacuum giving a 46% yield (basing on Ru).

Anal. Calcd. for $C_{17}H_{30}O_{18}Ru_3$: C, 24.64%; H, 3.62%. Found: C, 24.5%; H, 3.6%. IR (KBr disks): 1594s, 1511w, 1423s, 1373w, 1332w, 1297m, 1222w, 1045w, 929w, 784m, 767m, 727w, 526m cm^{-1}.

2.3. *Synthesis of $[Ru_3^{(II,III,III)}O(CH_3CO_2)_6(H_2O)_3]\cdot 2H_2O$ (**2**)*

For the preparation, 0.83 g (1 mmol) of **1** and 0.02 g (0.1 mmol) of muccic acid ($C_6H_{10}O_8$) were mixed in 10 mL of distilled water. Then the reaction mixture was stirred at room temperature to complete dissolving of chemicals, transferred in a Teflon-lined stainless vessel (40 mL) and heated at 180 °C for 72 h under autogenous pressure. After, the reaction was cooled down to room temperature, and resulted solid was filtered, washed several times with ice-cold distillated water and air-dried. The yield of dark green solid lustrous solid was 0.144 g (66%).

Anal. Calcd. for $C_{12}H_{28}O_{18}Ru_3$: C, 18.87 %; H, 3.67%. Found: C, 18.9%; H, 3.7%.

2.4. *Single-crystal X-ray diffraction and structure determination of **2***

Single-crystal X-ray diffraction data collection was performed at 293 K and 100 K on Oxford-Diffraction-Gemini diffractometer with a monochromatic CuKα radiation source (λ = 1.5418 Å). The CrysAlisPro program was used for cell refinement and data reduction. Images were collected at a 55 mm fixed crystal-detector distance, using the oscillation method, with 1° oscillation and variable exposure time per image. The structures were solved by direct methods using the SIR92 program [25]. The refinement was performed by SHELX-97 using full-matrix least squares on F^2 [26]. All non-H atoms were anisotropically refined except two crystallization

water molecules which were treated isotropically. Position of the H atoms were calculated based on geometric criteria (C-H = 0.96 Å for methyl groups) than have been placed in their calculated position and refined isotropically using a rider model with $U_{iso}(H) = 1.5\ U_{eq}(C)$ for methyl group. An absorption correction was performed using XABS2 program [27]. All intra- and inter-molecular interactions were found by PARST [28] and PLATON [29] program packages. Crystallographic data for **2** have been deposited to Cambridge Crystallographic Data Center with CCDC# 813218–813219 and can be obtained free of charge upon request at www.ccdc.cam.ac.uk/data_request/cif. Crystal data and structure refinement details for **2** at 293 K and 100 K are presented in Table 1.

Table 1. Crystallographic data and structure refinement for $[Ru_3(CH_3CO_2)_6(H_2O)_3]\cdot 2H_2O$ (**2**)

Temperature	**293 K**	**100 K**
Formula	$C_{12}H_{28}O_{18}Ru_3$	$C_{12}H_{28}O_{18}Ru_3$
Formula weight / g·mol^{-1}	763.55	763.55
Wavelength	CuKα (1.54184 Å)	CuKα (1.54184 Å)
Crystal system	Monoclinic	monoclinic
Space group	*C2/c*	*C2/c*
Unit cell dimensions		
a / Å	27.032(6)	26.923(9)
b / Å	13.832(3)	13.841(3)
c / Å	15.257(4)	15.165(6)
α / °	90	90
β / °	123.62(3)	123.13(5)
γ / °	90	90
Cell volume / Å^3	4751(3)	4732(4)
Z	8	8
Calc. Density / mg·m^{-3}	2.115	2.135
Absorption coefficient / mm^{-1}	16.01	16.07
F(000)	3008	2928
Crystal size / mm^3	0.03 × 0.06 × 0.08	0.07 × 0.06 × 0.01
Theta range for data collection / °	3.8 to 71	3.5 to 71.9
Index ranges	$-32\leq h \leq 33$, $-16\leq k \leq 14$, $-18\leq l \leq 18$	$-30\leq h \leq 33$, $-17\leq k \leq 14$, $-18\leq l \leq 15$
Reflection collected	19481	8935
Independent reflections	4541 [R_{int} = 0.04]	4405[R_{int} = 0.121]
Completeness to θ=70°	99 %	99 %
Absorption corrections	Empirical	Empirical
Max. and min. transmission	0.590 and 0.350	0.373 and 0.852
Refinement method	Full-matrix least-squares on F^2	Full-matrix least-squares on F^2
Data/restraints/parameters	4541/0/308	4405/0/288
Goodness-of-fit on F^2	0.901	0.972
Final R indices [$I>2\sigma(I)$]	R_1 = 0.049, wR_2 = 0.117	R_1 = 0.088, wR_2 = 0.203
R indices (all data)	R_1 = 0.084, wR_2 = 0.130	R_1 = 0.204, wR_2 = 0.293
Largest diff. peak and hole	1.35 and -0.72 e·Å^{-3}	1.17 and -1.05 e·Å^{-3}

$R_1 = \Sigma\ ||F_0| - |F_c|| / \Sigma\ |F_0|$ for observed data ($I > 2\sigma(I)$); number in parentheses is for all data.
$wR_2 = \{\Sigma\ [w(F_0^2 - Fc^2)^2] / \Sigma\ [w(F_0^2)^2]\}^{1/2}$ for observed data ($I > 2\sigma(I)$); number in parentheses is for all data.

2.5. *Characterization methods*

Microanalyses were carried out using a Perkin-Elmer model 2400B elemental analyzer. The IR spectra were recorded on a Bruker Tensor-27 spectrophotometer as KBr pellets in the 4000–400 cm^{-1} region. A Mettler-ToledoTGA/SDTA851 were used for the thermal analyses in nitrogen dynamic atmosphere (50 mL/min) at a heating rate of 10 °C/min. Approximately 10 mg of powder sample was thermally treated, and blank runs were performed.

X-ray microanalysis (SEM/EDX) confirmed composition of $[Ru_3^{(II,III,III)}O(CH_3CO_2)_6(H_2O)_3]\cdot 2H_2O$, by using JEOL JSM-6100 scanning microscopy (SEM) coupled with an INCA Energy-200 dispersive X-ray microanalysis system (EDX) with a PentaFET ultrathin window detector. As shown in Fig. S1 (Supplementary Materials), the lustrous dark green powder of **2** consists of macro-sized crystals exhibiting prismatic habit.

X-Ray powder diffraction patterns were collected with a X´Pert Philips X-ray diffractometer (CuK_α radiation, λ = 1.5418 Å) at room temperature. The powder diffraction analysis indicate that synthesized compound **2** show analogous pattern as for simulated from the atomic coordinates of **2** determined by single-crystal X-ray diffraction (Fig. S3, Supplementary Materials). X-ray near-edge absorption spectra (XANES) at Ru *K*-edge were recorded in transmittance mode at European Synchrotron Radiation Facility (ESRF, Grenoble) in Beamline BM25. The excitation energy was selected using a Si(111) double-crystal monochromator. The beam size of 1 mm (horizontal) × 1 mm (vertical) was controlled with a slit. The XANES spectra were measured on pallets containing approximately 40 mg of solid compound **2** in 200 mg of boron nitride. Each spectrum was recorded with 0.25 eV step size. All spectra processing procedures (i.e., normalization, smoothing, background subtraction and windowing) including linear combination calculations were done in the IFEFFIT software package [30, 31].

2.6. Catalytic experiments

Hydration reactions were carried out in Schlenk tube under N_2 atmosphere. The reaction mixture was prepared dissolving 5 mg (6.5 μmol) of catalyst **2** in 3 mL of H_2O. The mixture was degassed and 1.5 mmol of corresponding acetonitrile substrate was added with micropipette to stirred solution. The reaction was allowed for heating at 110 °C using oil bath or microwave-assisted heating. The isomerization reactions of allylic alcohols were conducted Schlenk tube under N_2 atmosphere. The reaction mixture was prepared dissolving 3 mg (3.9 μmol) of catalyst **2** in 2 mL of appropriate solvent (DMF, EtOH or H_2O). The mixture was degassed and 1 mmol of corresponding allylic alcohol substrate was added with micropipette to stirred solution. The reaction was allowed for heating using oil bath

The reaction solutions were analyzed by regular sampling using GC/FID (Hewlett Packard) equipped with Beta DEX 120 (30 m × 0.25 mm × 0.25 μm) 30 m long column. The degrees of conversion were calculated on the basis of the ratio of areas of the substrate material and the products determined from corresponding chromatograms. The optimization of chromatographic methods and the calibration procedures for detection of products as well as substrates were realized by injection of authentic commercial samples.

3. Results and Discussion

*3.1. Crystal structure of $[Ru_3O(CH_3CO_2)_6(H_2O)_3]\cdot 2H_2O$ (**2**)*

The single-crystal X-ray diffraction analysis reveals that compound **2** crystalizes in monoclinic space group *C*2/*c* with unit cell parameters listed in Table 1. The molecular structure of the acetate complex **2** is depicted in Figure 1. The asymmetric unit of 2 contains three crystallographically independent ruthenium atoms, one μ_3-oxygen, six acetate ligands, three coordinated and two lattice water molecules.

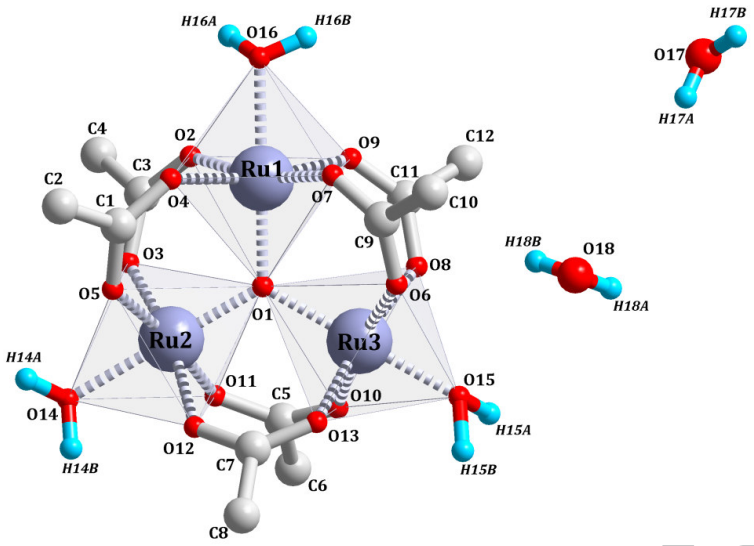

Figure 1. (*single column fitting image*) Molecular structure of complex **2** represented with corresponding atom labeling scheme. H atoms from the methyl groups were omitted for clarity.

As shown in Fig. 1, the three ruthenium atoms form a near to the equilateral triangle where pseudo-C_3 axis pass through μ_3-O perpendicular to the Ru–Ru plane with Ru···Ru separation distances of 3.322 and 3.274 Å. In similar way, three coordinated water molecules are located in the same plane that defines for Ru atoms. The central μ_3-O1 atom is located in the Ru_3 triangular plane near to the center of the triangle. The acetate ligands deviate from Ru_3 triangular plane on the angle of 45.2°. Furthermore, each ruthenium atom is in distorted octahedral coordination geometry formed by four carboxyl oxygen atoms originated from four different acetate ligands, one μ_3-O and one oxygen atom coming from coordinated water molecule. The average bond length of Ru-O is varied from 1.875(6) Å to 2.128(7) Å and depends from the temperature of measurement. Selected bond distances for ruthenium coordination environments in **2** at 100 K and 293 K are summarized in Table S1 (Supplementary Materials).

The crystal packing of **2** stabilized through multiple hydrogen bonds involving the coordinated water in $[Ru_3O(CH_3CO_2)_6(H_2O)_3]$ complex and two crystallization water molecules. There obviously exists strong intermolecular interaction in the hydrogen-bonding network associated with the valence state conversion. In the complex **2**, a calculation of intermolecular contacts suggests five hydrogen bonds listed in Table 2.

Table 2. Hydrogen bonds geometry* in structure of **2**

D*–H···*A	**d (*D*–H), Å**	**d (H···*A*), Å**	**d (*D*···*A*), Å**	**∠(*D*–H···*A*), °**
O14–H14A···O13	0.90	2.09	2.996(12)	179
O15–H15B···O5	0.90	2.09	3.145(17)	168
O16–H16B···O9	0.89	2.23	3.044(13)	152
O18–H18A···O17	0.89	1.93	2.69(4)	148
O18–H18B···O8	0.89	2.57	3.39(3)	161

*The hydrogen bonds were considered according to [32, 33]

The O18–H18B···O8 hydrogen bond holds one crystalized water molecule near to Ru3 site, while intermolecular O14–H14A···O13, O15–H15B···O5 and O16–H16B···O9 contacts contribute to the strengthen of cluster molecules packing (Fig. S4). Moreover, the hydrogen

bonds between individual cluster molecules connect the neighboring $[Ru_3O(CH_3CO_2)_6(H_2O)_3]$ complexes to construct a 2D framework. Better insight of resulted packing network can be achieved by topological analysis using TOPOS4.0 program package [34]. As shown in Fig. S5, each ruthenium oxo-cluster is linked to six equivalent neighbors *via* hydrogen bonds and represents a 6-connected node. The resulted non-interpenetrating 6-connected unimodal net is simplified as well-known Shubnikov hexagonal plane net topology (***hcb***) with the Schläfli symbol of (6,3) and the 6.6.6. vertex symbol.

3.2. Ruthenium mixed valence delocalization in $[Ru_3^{(II,III,III)}O(CH_3CO_2)_6(H_2O)_3]\cdot 2H_2O$

The formulation of $[Ru_3O(CH_3CO_2)_6(H_2O)_3]\cdot 2H_2O$ determined by single-crystal X-ray study implies that the ruthenium atoms in complex **2** are in mixed oxidation state with Ru^{II}:Ru^{III} ratio equal to 1:2. As have been observed in similar trinuclear-oxo compounds, where transition metal centers are found in mixed oxidation states, the resonant mixed valence delocalization between those three centers is usually occurred at room temperature [35-37]. The geometry of the coordination sphere around the transition metal centers atoms provides much more information about the oxidation state of these atoms and the degree of valence delocalization in the M_3O core [38-40]. In particular, the Ru–μ_3O distance and angles analysis are expected to be useful for determination of formal valences at each ruthenium center in $[Ru_3O(CH_3CO_2)_6(H_2O)_3]\cdot 2H_2O$ complex. Thus, the Ru–μ_3O distance and angles in Ru_3O triangular core were analyzed using single-crystal X-ray diffraction data measured at 293 K and 100 K. As shown in Fig. 2a, the Ru2–μ_3O bond length (1.875 Å) is significantly shorter than Ru1–μ_3O (1.905 Å) and Ru3–μ_3O (1.9931 Å), suggesting that Ru2 center is likely exhibit 3+ oxidation state.

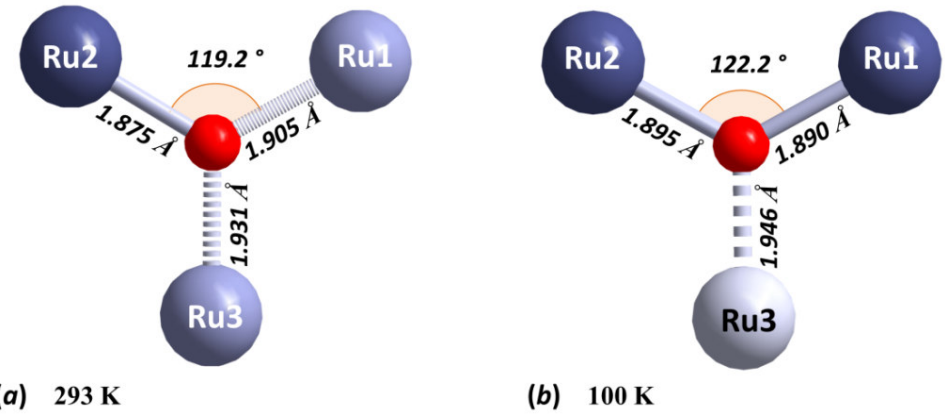

Figure 2. (*two column fitting image*) The Ru–μ_3O bond lengths and Ru2–O–Ru1 angle in triangular Ru_3O core of 2 as determined from single-crystal X-ray diffraction data at (a) 295 K and (b) 100K.

Furthermore, the Ru3–μ_3O appears to be longer than Ru1–μ_3O that is within the range as expected for the Ru(2+) atom. Meanwhile, intermediate position of Ru1–μ_3O bond points to the valence delocalization at Ru1 center. To support this, charge ordering calculation performed using VaList program [41], suggest that Ru2 atom site is mainly Ru(3+) while the Ru1 and Ru3 centers exhibit mixed valence state resembling charges of 2.3+ and 2.7+, respectively. This result indicate that the mixed oxidation delocalization take place between Ru1 and Ru3 at room temperature, where Ru1 atom site trend to Ru(2+) approximation. In contrast, as shown in Fig. 2b, at lower temperature Ru2–μ_3O and Ru1–μ_3O bond are close to be equal with lengths of 1.895

Å and 1.890 Å, respectively, while Ru3–μ_3O bond become larger (1.946 Å). Moreover, the Ru2–μ_3O–Ru1 is also depended on the valence state and, as shown in Fig. 2, upon temperature decreasing became larger on 3°. These observations indicate that oxidation state trapping (3+) on Ru1 center occurs at lower temperatures. As supported by valence bond calculation at 100 K, the ruthenium site oxidation for Ru1 and Ru2 metal centers are 3+ whereas for Ru3 center calculated value became Ru(2+).

In order to confirm the mixed oxidation states of ruthenium atoms in oxo-cluster **2**, the XANES technique was applied. The normalized XANES spectra for solid samples of **2** and reference compounds measured on Ru K adsorption edge are shown in Fig. 3.

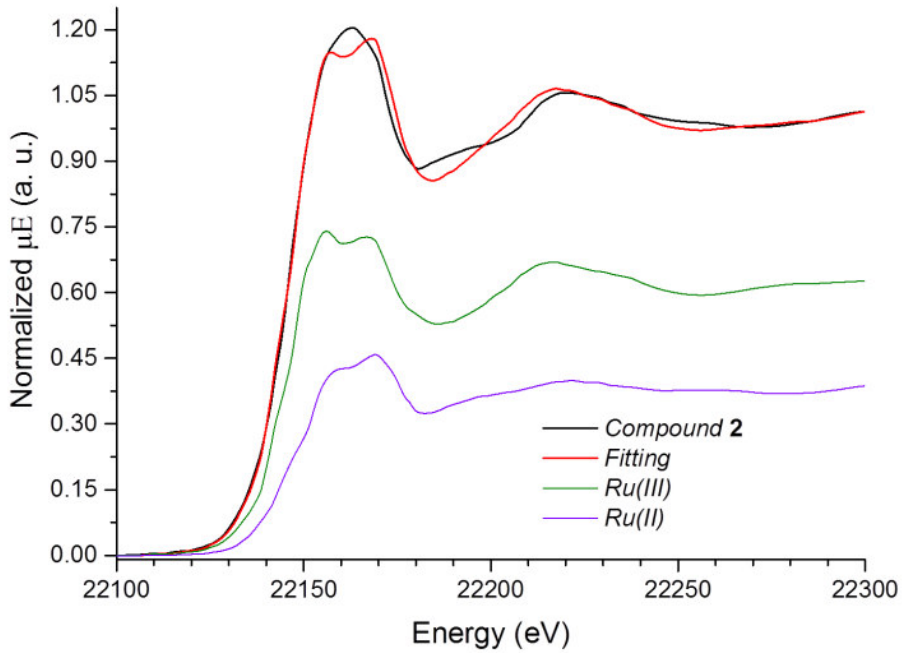

Figure 3. (*single column fitting image*) XANES part of the Ru K-edge X-ray absorption spectra of compound **2** with corresponding fitting plot realized using the absorption edges positions of reference compounds Ru(III) and Ru(II) as a calibration data for determination of Ru formal oxidation states in oxo-cluster **2**.

The adsorption edges (determined from the derivatives of normalized spectra) were used to estimate the formal oxidation state of ruthenium atoms in triruthenium oxo-cluster **2**. As follows from fitting data represented in Fig. 3, the $[Ru_3^{(II,III,III)}O(CH_3CO_2)_6(H_2O)_3]\cdot 2H_2O$ complex have the position of the Ru absorption K-edge E_o close to 22142 eV. A combination fit of the experimental data using the E_o values of corresponding Ru(III) and Ru(II) reference compounds suggests that the ruthenium centers in complex **2** exhibit II-III mixed valance state. The Ru^{II}:Ru^{III} ratio of formal oxidation states for three ruthenium centers is found to be 0.38:0.62 (calc. 0.33:0.67) which is consistent with expected for $Ru^{II}Ru_2^{III}$ core.

The magnetic nature of the analogous triruthenium oxo-complex has been previously discussed by Cotton and Norman [10]. According to this work the mixed-valence $Ru^{II}Ru_2^{III}$ oxo-bridged complex exhibits diamagnetic properties even though the Ru(III) centers possess unpaired electrons. That can be better explained by a molecular orbital treatment of the entire Ru_3O-core rather than considering the Ru(III) centers separately: 16 electrons of Ru_3O are paired in bonding and nonbonding orbitals resulting in diamagnetic complex.

3.3. *Thermogravimetric analysis*

The thermal stability of **2** in nitrogen atmosphere was investigated. As shown in Figure 4, where corresponding TG/DTG curves are presented, decomposition of ruthenium oxo-cluster proceeds through three steps with total mass loss of 58.4%. The first step, which take place in temperature range of 60–200 °C with maximum velocity at 130 °C and has endothermic effect in SDTA curve, reveals mass loss of 9.4 % and corresponds evacuation of 4 moles (calc. 9.43%) of water molecules (two crystallization and two coordinated water).

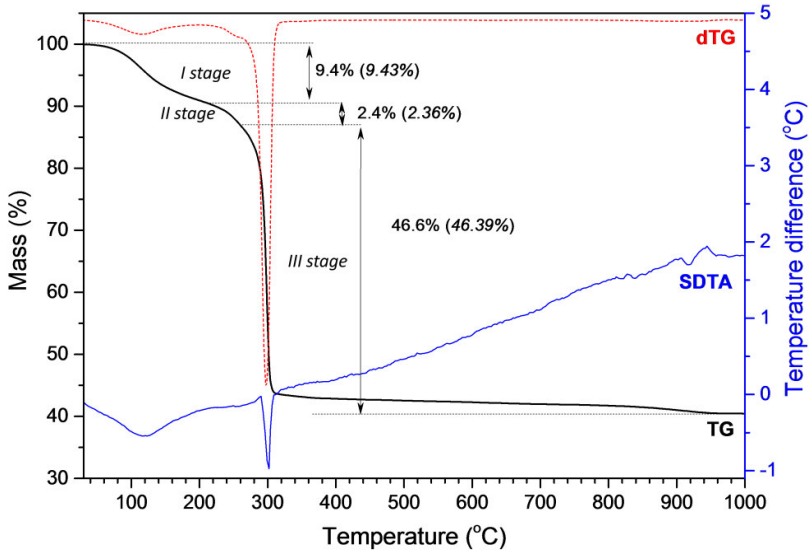

Figure 4. (*single column fitting image*)Thermogravimetric (TG), derivative (dTG) and simultaneous differential thermal analysis (SDTA) curves corresponding to decomposition profile of **2** in nitrogen atmosphere.

The second mass loss step is partially overlapped with third stage and occurred between 240 and 280 °C reaching maximum velocity at 260 °C. The mass loss corresponding to this stage is 2.4% followed by endothermic peak in SDTA graph and attributed to the loss of one remaining coordinated water molecule (calc. 2.36 %). The third step occurred in the range of temperatures 290–400 °C with maximum velocity at 300 °C and the mass loss of 46.6% is associated with decomposition of acetate ligands in resulted anhydrous acetate oxo-cluster (calc. 46.39%). Assuming that decomposition of **2** take place in inert nitrogen atmosphere, metallic ruthenium is expected as final product of pyrolysis that leads to the residue mass of 41.6 % (calc. 41.07%).

3.4. *Infrared spectroscopic characterization*

The infrared spectrum of complex **2** acquired from 4000 cm^{-1} to 400 cm^{-1} is dominated by vibrational modes involving the bridging acetate group (Fig. S6a). The high-energy, relatively weak bands observed ~ 2925 cm^{-1} are attributed to C–H stretching of acetate ligands, while the methyl bending mode is represented by peak centered at 1354 cm^{-1}. Other bands occurred at 948 cm^{-1} and 686 cm^{-1} apparently attribute to acetate ligands [3]. The intense peaks located at 1630 cm^{-1} and 1572 cm^{-1} are associated to asymmetric carboxylate stretching frequencies, whereas the lower energy band ~1429 cm^{-1} is due to symmetric stretching of carboxylic group [42]. Furthermore, the bands observed at 1039 cm^{-1} and 619 cm^{-1} were assigned to (μ_3-O)–Ru bridging vibrations in complex **2** [43].

Vibration modes of coordinated water molecules occur in the region 3600–3300 cm^{-1}, among the peak centered at 3550 cm^{-1} corresponds to crystallized water molecules [42]. Interestingly, when the complex **2** was heated at 140 °C under vacuum during 3 hours, the dehydration of ruthenium oxo-cluster is occurred as was evidenced by disappearance of the broad peak in the region of 3600–3300 cm^{-1} (Fig. S6b). Moreover, the bands attributed to variations of carboxyl groups are slightly shifted to 1537 cm^{-1} and 1410 cm^{-1} indicating that the polarity of $Ru–O_{carboxyl}$ bond increase as a result of releasing coordinated water molecules out of ruthenium coordination sphere.

*3.5. Catalytic activity of **2** in hydration of nitriles to amides in aqueous medium*

Hydration of nitriles is one of the most important reaction applied for industrial purposes since its form inherent link in the large-scale production of amines, which are synthetic intermediates used in manufacture of pharmacological products, polymers, detergents, etc [44]. To this regard, a variety of ruthenium-based complexes able to selectively and efficiently catalyze hydration of nitriles to amides in aqueous media have been reported [45-47]. Basing on these precedents, the trinuclear oxo-cluster **2** was examined in nitrile hydration reaction. In a typical experiment, 1.5 mmol% of **2** was dissolved in 3 mL of H_2O and 1.5 mmol of corresponding acetonitrile substrate was added. The reaction mixtures were allowed for heating at 110 °C using oil bath or microwave-assisted heating.

As shown in Table 3, the triruthenium oxo-cluster **2** was found to be active catalyst, reaching amides formation with yields up to TOF of 248 h^{-1}. It worth to noting that the activity of complex **2** is higher and more pronounced when reaction was assisted by microwave heating. Comparing to the nitriles conversions obtained using conventional heating, which are usually occurred from 5 to 50 h, the microwave-assisted transformation was much faster reaching high conversion percentage in less than two hours.

In order to explore the effect of hydrophobicity of the substrate on the course of hydration of nitriles in aqueous media, we focused on the wide array of aliphatic nitriles with different chain lengths. Thus, as observed in entries 1a-d, the TOF values corresponding to conversions of different substrates increases as the aliphatic chain length increases. Since the solubility of those aliphatic nitriles in aqueous media drastically decreases as the aliphatic chain growth, it is reasonable to conclude that the hydration reaction is favorable biphasic.

As expected, the hydration reaction course should vary somewhat depending on the reactivity of the nitrile. Using the same reaction conditions a wide range of nitriles substrates was examined, i.e.: benzonitrile, hexanenitrile, phenoxyacetonitrile, 3-chlorbenzonitrile, methylbenzonitrile and 3-nitrobenzonitrile. As shown in Fig. S7, the kinetic plots for the studied substrates exhibit different slopes featuring variable reactivity. Summarizing, the order of reactivity of nitriles is benzonitrile > 3-nitrobenzonitrile > phenoxyacetonitrile > 3-chlorbenzonitrile > hexanenitrile > 3-methylbenzonitrile. The same order of reactivity is observed upon microwave-assisted heating, as shown in and Table 3 (entries 1d, 2a, 2c, 3a, 4b and 6a-b). Also, the reactivity of benzonitrile as a function of electron-withdrawing groups was studied. Thus, comparing the conversion rates for methyl-, nitro-, chlor- and methoxy-substituted in ortho-position benzonitriles (entries 2c, 3a, 4b and 5b), the reactivity of the substrates fall in order of Cl > NO_2 > CH_3 > OCH_3 that is also confirmed by results obtained in microwave-assisted experiments. In other hand, beside to consequence of electron-withdrawing power of the substituents, the position of these groups is also expected to affect the reactivity of the substrates.

Table 3. Hydration of nitriles in aqueous mediuam catalyzed by triruthenium oxo-cluster **2** at 110 °C

Entry	Substrate	Product	Conventional heating [a]			Microwave-assisted heating [b]		
			time, h	yield, %	TOF, h^{-1}	time, h	yield, %	TOF, h^{-1}
1a		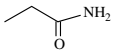	47	59	3.1	2	28	35
1b	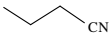	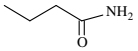	13	45	8.6	2	65	81
1c	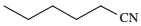	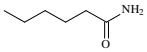	14	87	15.5	2	92	115
1d	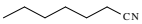	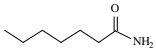	7	92	32.9	1	78	195
2a		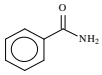	6.5	97	37.3	1	97	242
2b		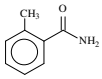	27	64	5.9	2	41	51
2c	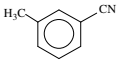	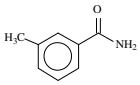	11	57	12.9	2	76	95
2d	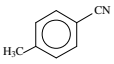	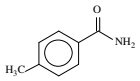	17	92	13.5	1.5	94	156.7
3a	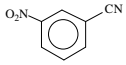	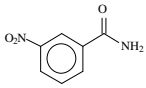	9	94	26.1	1	92	230
4a		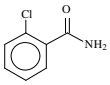	18	85	23.6	1	86	215
4b	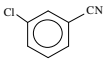	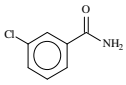	7	87	31.1	1	99	247.5
4c	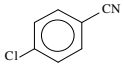	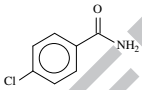	6	97	40.4	1	99	247.5
5a	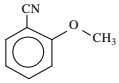	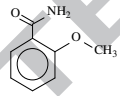	50	51	2.6	4	61	38.1
5b	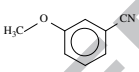	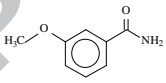	40	72	4.5	2	88	110
5c	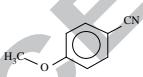	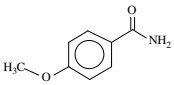	13	99	19	1	93	232.5
6a	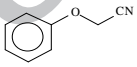	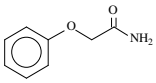	12	92	19.2	1	82	205
6b	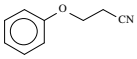	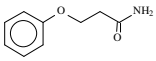	9	98	27.2	1	99	247.5
			Recycling tests					
7a		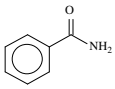	–	–	–	1	96	222
7b		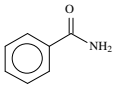	–	–	–	1	96	222

[a] Reaction performed under N_2 atmosphere at 110 °C in Schlenk tube using 1.3 mmol% (Ru) of catalyst, 1.5 mmol of substrate and 3 mL H_2O.
[b] Reaction performed under N_2 atmosphere at 110 °C in microwave autoclave using the same conditions as for ***a***.
TOF = mmol of product / mmol of catalyst (basing on Ru) / hours.

As resulted from the data in Table 3 corresponding to entries 2c-d (for methyl-group), 4a-c (for chlor-group) and 5a-c (for methoxy-group), ortho-substituted substrates showed a lower reactivity compared to their meta- or para-substituted counterparts (entry 2b *vs* 2b-c, entry 4a *vs* 4b-c, 5a *vs* 5b-c) which is likely due to steric factors.

In overall, the reactivity of the substrates follows the order of para > meta > ortho perceiving particular electron-withdrawing effects of each sort of substituent group.

The recyclability tests for complex **2** have been performed using benzonitrile as a model substrate. The catalytic system contained **2** was allowed to react with benzonitrile for 1 h under microwave heating at 110 °C, then reaction mixture was cooled to 10°C for quantitative separation of crystalline benzamide product. After, the aqueous solution contained dissolved oxo-cluster **2** was removed by decantation and reused for next catalytic run through adding a new portion of benzonitrile (Fig. S8). As shown in Table 3 (entries 2a, 7a-b), the catalytic activities of **2** along three consecutive cycles (2a: 1st, 7a: 2nd, 7b: 3rd run) is remain almost constant leading to conversions of 96% in 1 h (TOF = 222 h^{-1}). These observations suggest that acetate triruthenium oxo-cluster **2** remain catalytic activity upon at least three consecutive cycles.

*3.6. Catalytic activity of **2** in isomerization of allylic alcohols*

The high catalytic activities of rhodium oxo-complex selective isomerization of allylic alcohols early reported by Morrill and Grubbs [48], and similarity in the catalytic behavior of ruthenium-based compounds [49-51], motivated us for realizing the catalytic tests of ruthenium oxo-cluster **2** in this organic transformation. In typical experiment, the ruthenium complex **2** (1.2 mmol% Ru) was dissolved in appropriate solvent and 1 mmol of allylic alcohol substrate was added. The results of catalytic tests performed with ruthenium complex **2** are summarized in Table 4. A set of variables were examined in order to optimize reaction conditions. The first variable was a temperature (Table 4, entries 1b, 4a-c). The 1-penten-3-ol was chosen as a model substrate. It was observed that the catalytic activity of **2** decreases as the temperature increases, and the higher performance with TOF of 1.7 h^{-1} is stabilized at 80 °C. Therefore, this temperature was used as an optimal for the next set of experiments.

The earliest study of Peterson and Larock [52], focused on the isomerization of primary and secondary allylic alcohols, demonstrates considerable improvement of catalytic activities upon addition of base, i.e. $NaHCO_3$. Thus, in order to evaluate the effect base, the corresponding tests were conducted with $NaHCO_3$, KOH and without additive (Table 4: entry 1e, 5a and 5b, respectively). Unsatisfactory conversion was obtained in experiment 5b, where the isomerization reaction was realized at 80 °C without the base. Meanwhile, the addition of KOH improves isomerization of 1-octen-3-ol to 3-octanone reaching TOF of 0.01 h^{-1}. The best catalytic performance of **2** has been obtained with addition of $NaHCO_3$ (TOF 1.7 h^{-1}).

Using the optimized catalytic conditions, the next task was to determinate the effect of solvent. A series of substrates (i.e.: 3-buten-2-ol, 1-penten-3-ol, 1-hexen-3-ol, 1-hepten-3-ol and 1-octen-3-ol) was examined with three commonly employed solvents (Table 4: entries 1a-e, 2a-e, 3a-e). A survey of the results show that the use of water as reaction medium don't favor the isomerization reaction and the catalytic activity decreases as the length of aliphatic chain of the substrate increases. As expected, the hydrophobicity of substrate alcohols increase in order 3-buten-2-ol > 1-penten-3-ol > 1-hexen-3-ol > 1-hepten-3-ol > 1-octen-3-ol, that stimulate the aqueous reaction solution to became a inhomogeneous biphasic mixture and lead to worsening of interactions between substrate and dissolved homogeneous catalyst.

Table 4. Isomerization of allylic alcohols catalyzed by triruthenium oxo-cluster **2**

Entry	Substrate	Product	Solvent	Base	T, °C	*t*, h	yield, %	TOF, h^{-1}
1a						45	97	1.8
1b	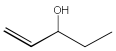	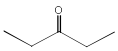				47	95	1.7
1c	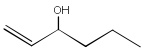	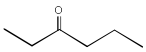	DMF	$NaHCO_3$	80	41	86	1.7
1d	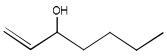	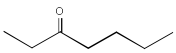				41	96	1.9
1e	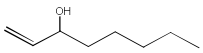	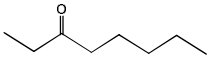				65	67	0.9
2a						23	94	3.4
2b	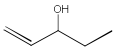	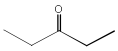				23	96	3.5
2c	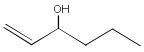	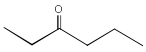	EtOH	$NaHCO_3$	80	30	74	2.1
2d	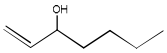	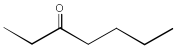				71	38	0.4
2e	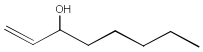	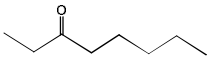				60	95	1.3
3a						48	5	0.1
3b	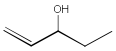	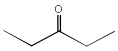				24	2	0.1
3c	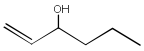	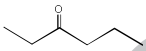	H_2O	$NaHCO_3$	80	12	1.5	0.1
3d	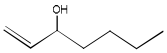					24	0	0
3e	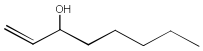					24	1	0.03
4a	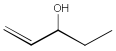	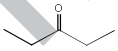			RT	48	0.6	0.01
4b	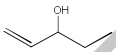	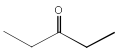	DMF	$NaHCO_3$	65	71	6.5	0.01
4c	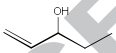	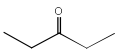			100	26	51	1.6
5a	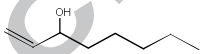	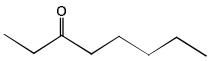	DMF	KOH	80	24	1	0.03
5b	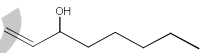	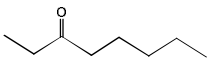		–	80	72	0	0

Reaction performed under N_2 atmosphere in Schlenk tube using 1.2 mmol% (Ru) of catalyst and 1 mmol of substrate. TOF = mmol of product / mmol of catalyst (basing on Ru) / hours.

In contrast, the use of DMF as the solvent led to almost complete conversion of the started alcohol and afforded desired ketone with yields up to 97% (TOF of 1.8 h^{-1}). Notably, that effect of reactivity of alcohol substrate as a function of length of aliphatic chain is not observed with DMF solution, which is reasonable considering that the DMF is one of the best solvents for variety of chemical substances. Finally, as expected the highest catalytic performances of **2** were obtained with ethanol as reaction solvent reaching TOF values up to 3.5 h^{-1} (Table 4: entries 2a-e).

4. Conclusions

The trinuclear ruthenium-oxo cluster $[Ru_3^{(II,III,III)}O(CH_3CO_2)_6(H_2O)_3]\cdot 2H_2O$ (**2**) firstly has been prepared with high yield by one-electron reduction of $[Ru_3^{(III,III,III)}O(CH_3CO_2)_6(CH_3OH)_3]\cdot CH_3CO_2$ precursor **1** using muccic acid as reductor under hydrothermal conditions at 180 °C. Single-crystal X-ray analysis reveals that synthesized compound **2** is mixed-valence oxo-centered trinuclear ruthenium acetate complex where oxidation state delocalization at room temperature between one Ru^{III} and one Ru^{II} sites are postulated basing on the precise analysis of crystallographic data and valence bond calculations. Furthermore, the mixed-valence states in Ru^{II}–μ_3O–Ru_2^{III} structural unit have been confirmed basing on the XANES spectral analysis of $[Ru_3^{(II,III,III)}O(CH_3CO_2)_6(H_2O)_3]\cdot 2H_2O$.

The crystal structure of **2** displays 2D supramolecular networks extended through multiple hydrogen bonds which can be simplified to hexagonal plane (***hcb***) topological net. Moreover, triruthenium oxo-cluster **2** is thermally stable up to 250 °C, and its molecular structure remains unchanged upon dehydration.

The catalytic tests performed for hydration of nitriles in water medium reveal that oxo-cluster **2** shows to be active homogeneous catalyst in this transformation reaching conversions up to 99%. Notably, the highest catalytic performances were obtained under experimental sets where heating have been assisted by microwaves. The evaluation of activity of various nitrile substrates suggests that hydration of nitriles is likely biphasic and follow the order of benzonitrile > 3-nitrobenzonitrile > phenoxyacetonitrile > 3-chlorbenzonitrile > hexanenitrile > 3-methylbenzonitrile. In addition, the nature of electron-withdrawing group as well as its position also shows to affect the reaction efficiency, and the catalytic activity was decreasing in order Cl > NO_2 > CH_3 > OCH_3 and in sequence para > meta > ortho positions. Moreover, the recyclability tests for catalyst **2** reveal constant catalytic activity up to three consecutive runs.

Beside remarkable behavior of **2** in hydration of nitriles reaction, the triruthenium oxo-cluster shows to be active in isomerization of allylic alcohols reaction in presence of $NaHCO_3$. Under evaluation of reaction conditions we determine that optimal temperature for this organic transformation is 80 °C. The set of experiments suggest that the best conversions of variety of substrates were achieved using DMF as a solvent which is expected due to the miscibility effects. Furthermore, the substrate activity evaluations define order of 3-buten-2-ol > 1-penten-3-ol > 1-hexen-3-ol > 1-hepten-3-ol > 1-octen-3-ol.

***Acknowledgements*.** The authors thank FEDER and Spanish MINECO for financial support under projects MAT2013-40950-R, Consolider ORFEO. A.D. also thanks to Spanish *Ministerio de Educación, Cultura y Deporte* by their pre-doctoral FPU grant (AP2008-03942). The synchrotron measurement time was provided by ESRF (Grenoble, France) within the research project No. CH-3428. The authors thank staff members of BM25 (SpLine): Dr. Germán R. Castro, Dr. Iván Da Silva González and Dr. Pilar Ferrer Escorihuela for the technical support, guidance and useful suggestions on XANES data collection at the synchrotron facility.

Supporting Materials containes digital microgrphas of **1–8** crystal habits, SEM images, observed and calculated X-ray powder diffraction patterns, IR spectra, additional structure plots, kinetic plots for hydration of nitriles reaction and images of recyclability tests.

References

[1] M. Abe, Y. Sasaki, T. Yamaguchi, T. Ito, X-Ray Structure, Ligand Substitution, and Other Properties of Trinuclear Ruthenium Complex, $[Ru_3(\mu_3\text{-}O)(\mu\text{-}C_6H_5COO)_6(py)_3](PF_6)$ (py = pyridine), and X-Ray Structure of Dinuclear Ruthenium Complex, $[Ru_2(\mu\text{-}C_6H_5COO)_4Cl]$, Bulletin of the Chemical Society of Japan, 65 (1992) 1585-1590.

[2] O. Almog, A. Bino, D. Garfinkel-Shweky, The structure of oxo-bridged trinuclear ruthenium and iridium hexacarboxylates, Inorganica Chimica Acta, 213 (1993) 99-102.

[3] J.A. Baumann, D.J. Salmon, S.T. Wilson, T.J. Meyer, W.E. Hatfield, Electronic structure and redox properties of the clusters $[Ru_3O(CH_3CO_2)_6L_3]^{n+}$, Inorganic Chemistry, 17 (1978) 3342-3350.

[4] S. Davis, R.S. Drago, Synthesis, characterization, and oxidation catalysis by a novel (μ_3-oxo)triruthenium carboxylate complex, Inorganic Chemistry, 27 (1988) 4759-4760.

[5] A. Ohto, A. Tokiwa-Yamamoto, T. Ito, M. Abe, Y. Sasaki, K. Umakoshi, R.D. Cannon, Structure and vibrational spectra of trinuclear metal cluster complexes. A question of symmetry, Chemistry Letters, 26 (1995) 97-98.

[6] T.B. Rauchfuss, Ruthenium Complexes, Inorganic Syntheses, John Wiley & Sons, Inc.2010, pp. 148-163.

[7] A. Spencer, G. Wilkinson, μ-Oxo-triruthenium carboxylate complexes, Journal of the Chemical Society, Dalton Transactions, DOI 10.1039/DT9720001570(1972) 1570-1577.

[8] H.E. Toma, C.J. Cunha, C. Cipriano, Redox potentials of trinuclear μ-oxo ruthenium acetate clusters with N-heterocyclic ligands, Inorganica Chimica Acta, 154 (1988) 63-66.

[9] A. Spencer, G. Wilkinson, Reactions of μ_3-oxo-triruthenium carboxylates with π-acid ligands, Journal of the Chemical Society, Dalton Transactions, DOI 10.1039/DT9740000786(1974) 786-792.

[10] F.A. Cotton, J.G. Norman, Structural Characterization of a Basic Ruthenium Acetate, Inorganica Chimica Acta, 6 (1972) 411-419.

[11] C. Bilgrien, S. Davis, R.S. Drago, The selective oxidation of primary alcohols to aldehydes by oxygen employing a trinuclear ruthenium carboxylate catalyst, Journal of the American Chemical Society, 109 (1987) 3786-3787.

[12] S.A. Fouda, G.L. Rempel, μ_3-Oxo-triruthenium acetate cluster complexes as catalysts for olefin hydrogenation, Inorganic Chemistry, 18 (1979) 1-8.

[13] H.E. Toma, K. Araki, A.D.P. Alexiou, S. Nikolaou, S. Dovidauskas, Monomeric and extended oxo-centered triruthenium clusters, Coordination Chemistry Reviews, 219–221 (2001) 187-234.

[14] H.E. Toma, K. Araki, A.L.B. Formiga, A.D.P. Alexiou, G.S. Nunes, Electrocatalytic oxidation of methanol by the $[Ru_3O(OAc)_6(py)_2(CH_3OH)]^{3+}$ cluster: improving the metal-ligand electron transfer by accessing the higher oxidation states of a multicentered system, Química Nova, 33 (2010) 2046-2050.

[15] J.-L. Chen, X.-D. Zhang, L.-Y. Zhang, L.-X. Shi, Z.-N. Chen, Syntheses and Characterization of Oxo-Centered Triruthenium Compounds with Orthometalated Bipyridine, Inorganic Chemistry, 44 (2005) 1037-1043.

[16] Z.-N. Chen, F.-R. Dai, Oxo-Centered Triruthenium-Acetate Cluster Complexes Derived from Axial or Bridging Ligand Substitution, in: X.-T. Wu (Ed.) Controlled Assembly and Modification of Inorganic Systems, Springer Berlin Heidelberg2009, pp. 93-120.

[17] V. Guillerm, S. Gross, C. Serre, T. Devic, M. Bauer, G. Ferey, A zirconium methacrylate oxocluster as precursor for the low-temperature synthesis of porous zirconium(IV) dicarboxylates, Chemical Communications, 46 (2010) 767-769.

[18] M. Eddaoudi, D.B. Moler, H. Li, B. Chen, T.M. Reineke, M. O'Keeffe, O.M. Yaghi, Modular Chemistry: Secondary Building Units as a Basis for the Design of Highly Porous and Robust Metal–Organic Carboxylate Frameworks, Accounts of Chemical Research, 34 (2001) 319-330.

[19] A. Schoedel, M.J. Zaworotko, $[M_3(\mu_3\text{-}O)(O_2CR)_6]$ and related trigonal prisms: versatile molecular building blocks for crystal engineering of metal-organic material platforms, Chemical Science, 5 (2014) 1269-1282.

[20] U. Schubert, Cluster-based inorganic-organic hybrid materials, Chemical Society Reviews, 40 (2011) 575-582.

[21] D.J. Tranchemontagne, J.L. Mendoza-Cortes, M. O'Keeffe, O.M. Yaghi, Secondary building units, nets and bonding in the chemistry of metal-organic frameworks, Chemical Society Reviews, 38 (2009) 1257-1283.

[22] Y. Sasson, G.L. Rempel, Oxidative Transfer Dehydrogenation of α,β-Unsaturated Carbinols to α,β-Unsaturated Ketones Catalyzed by Ruthenium Complexes, Canadian Journal of Chemistry, 52 (1974) 3825-3827.
[23] Henrique E. Toma, Anamaria D.P. Alexiou, S. Dovidauskas, Extended Electronic Interactions in a Triangular μ-Oxotriruthenium Acetate Cluster Containing Nitric Oxide, European Journal of Inorganic Chemistry, 2002 (2002) 3010-3017.
[24] S.A. Fouda, B.C.Y. Hui, G.L. Rempel, Hydrogen reduction of μ_3-oxo-triruthenium(III) acetate in dimethylformamide, Inorganic Chemistry, 17 (1978) 3213-3220.
[25] A. Altomare, G. Cascarano, C. Giacovazzo, A. Guagliardi, M.C. Burla, G. Polidori, M. Camalli, SIR92 - a program for automatic solution of crystal structures by direct methods, Journal of Applied Crystallography, 27 (1994) 435.
[26] G. Sheldrick, Crystal structure refinement with SHELXL, Acta Crystallographica Section C, 71 (2015) 3-8.
[27] S. Parkin, B. Moezzi, H. Hope, XABS2: an empirical absorption correction program, Journal of Applied Crystallography, 28 (1995) 53-56.
[28] M. Nardelli, PARST95 - an update to PARST: a system of Fortran routines for calculating molecular structure parameters from the results of crystal structure analyses, Journal of Applied Crystallography, 28 (1995) 659.
[29] A. Spek, Structure validation in chemical crystallography, Acta Crystallographica Section D, 65 (2009) 148-155.
[30] M. Newville, IFEFFIT : interactive XAFS analysis and FEFF fitting, Journal of Synchrotron Radiation, 8 (2001) 322-324.
[31] B. Ravel, M. Newville, ATHENA, ARTEMIS, HEPHAESTUS: data analysis for X-ray absorption spectroscopy using IFEFFIT, Journal of Synchrotron Radiation, 12 (2005) 537-541.
[32] G.R. Desiraju, The C-H···O hydrogen bond in crystals: what is it?, Accounts of Chemical Research, 24 (1991) 290-296.
[33] G.R. Desiraju, The C–H···O Hydrogen Bond: Structural Implications and Supramolecular Design, Accounts of Chemical Research, 29 (1996) 441-449.
[34] V.A. Blatov, A.P. Shevchenko, D.M. Proserpio, Applied Topological Analysis of Crystal Structures with the Program Package ToposPro, Crystal Growth & Design, 14 (2014) 3576-3586.
[35] Y.-K. Lv, Y.-L. Feng, L.-H. Gan, M.-X. Liu, L. Xu, C. Liu, H.-W. Zheng, J. Li, Synthesis of Co-containing mesoporous carbon foams using a new cobalt-oxo cluster as a precursor, Journal of Solid State Chemistry, 185 (2012) 198-205.
[36] T. Sato, F. Ambe, An Oxo-Centered Trinuclear Cobalt(II)-Diiron(III) Acetate-Aqua Complex, Acta Crystallographica Section C, 52 (1996) 3005-3007.
[37] T. Sato, F. Ambe, K. Endo, M. Katada, H. Maeda, T. Nakamoto, H. Sano, Mixed-Valence States of $[Fe_3O(CH_2XCO_2)_6(H_2O)_3]\cdot nH_2O$ (X = H, Cl, and Br) Characterized by X-ray Crystallography and ^{57}Fe-Mössbauer Spectroscopy, Journal of the American Chemical Society, 118 (1996) 3450-3458.
[38] M. Manago, S. Hayami, Y. Yano, K. Inoue, R. Nakata, A. Ishida, Y. Maeda, Valence Delocalization and Crystal Structure of $[Fe_3O(pazo)_6(py)_3]\cdot 3py$: An Example of the Mixed Valence Delocalization between Two Iron Atoms, Bulletin of the Chemical Society of Japan, 72 (1999) 2229-2234.
[39] J. Overgaard, F.K. Larsen, B. Schiøtt, B.B. Iversen, Electron Density Distributions of Redox Active Mixed Valence Carboxylate Bridged Trinuclear Iron Complexes, Journal of the American Chemical Society, 125 (2003) 11088-11099.
[40] A.E. Tapper, J.R. Long, R.J. Staples, P. Stavropoulos, Oxygenation of Hydrocarbons Mediated by Mixed-Valent Basic Iron Trifluoroacetate and Valence-Separated Component Species under Gif-Type Conditions Involves Carbon- and Oxygen-Centered Radicals, Angewandte Chemie, 112 (2000) 2433-2436.
[41] A. Wills, VALIST. Program available from www.CCP14.ac.uk
[42] G. Socrates, Infrared and Raman characteristic group frequencies: Table and Charts, Ltd WJS, (2001) 1-347.
[43] K. Nakamoto, Infrared and Raman spectra of inorganic and coordination compounds, Wiley Online Library2009.

[44] T.J. Ahmed, S.M.M. Knapp, D.R. Tyler, Frontiers in catalytic nitrile hydration: Nitrile and cyanohydrin hydration catalyzed by homogeneous organometallic complexes, Coordination Chemistry Reviews, 255 (2011) 949-974.
[45] R. Garcia-Alvarez, P. Crochet, V. Cadierno, Metal-catalyzed amide bond forming reactions in an environmentally friendly aqueous medium: nitrile hydrations and beyond, Green Chemistry, 15 (2013) 46-66.
[46] R. García-Álvarez, J. Díez, P. Crochet, V. Cadierno, Arene−Ruthenium(II) Complexes Containing Amino−Phosphine Ligands as Catalysts for Nitrile Hydration Reactions, Organometallics, 29 (2010) 3955-3965.
[47] R. García-Álvarez, J. Díez, P. Crochet, V. Cadierno, Arene–Ruthenium(II) Complexes Containing Inexpensive Tris(dimethylamino)phosphine: Highly Efficient Catalysts for the Selective Hydration of Nitriles into Amides, Organometallics, 30 (2011) 5442-5451.
[48] C. Morrill, R.H. Grubbs, Highly Selective 1,3-Isomerization of Allylic Alcohols via Rhenium Oxo Catalysis, Journal of the American Chemical Society, 127 (2005) 2842-2843.
[49] V. Cadierno, P. Crochet, J. Gimeno, Ruthenium-Catalyzed Isomerizations of Allylic and Propargylic Alcohols in Aqueous and Organic Media: Applications in Synthesis, Synlett, 2008 (2008) 1105-1124.
[50] P. Lorenzo-Luis, A. Romerosa, M. Serrano-Ruiz, Catalytic Isomerization of Allylic Alcohols in Water, ACS Catalysis, 2 (2012) 1079-1086.
[51] B.M. Trost, R.J. Kulawiec, Chemoselectivity in the ruthenium-catalyzed redox isomerization of allyl alcohols, Journal of the American Chemical Society, 115 (1993) 2027-2036.
[52] K.P. Peterson, R.C. Larock, Palladium-Catalyzed Oxidation of Primary and Secondary Allylic and Benzylic Alcohols, The Journal of Organic Chemistry, 63 (1998) 3185-3189.

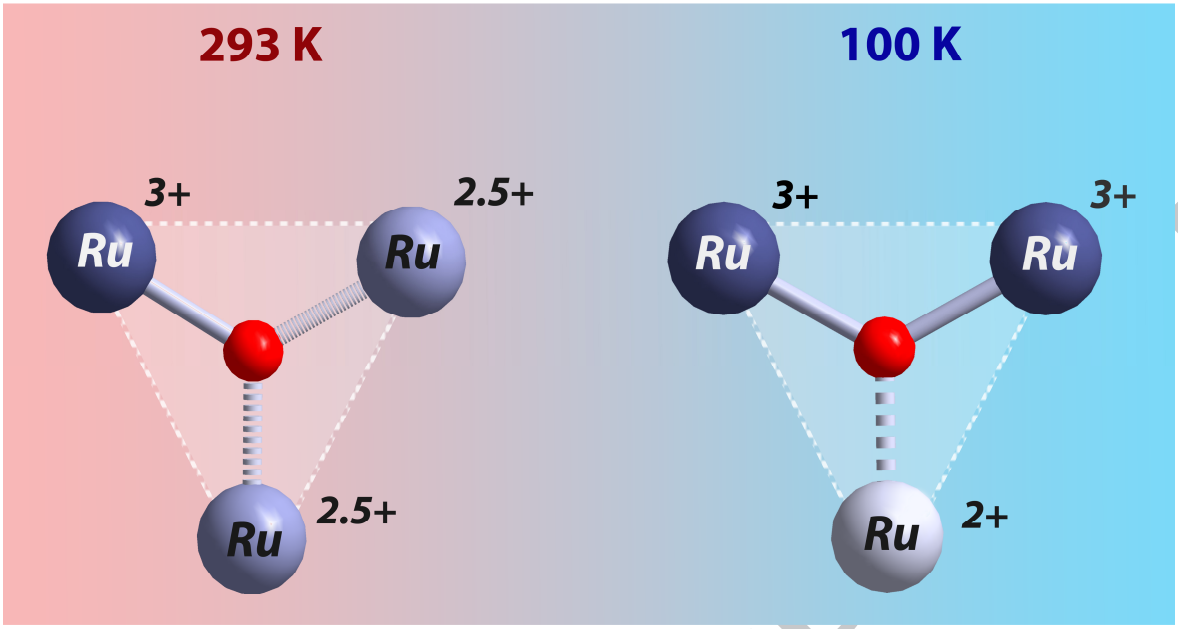

- The trinuclear ruthenium-oxo cluster was prepared under hydrothermal conditions.
- The crystal structure was determined basing on single-crystal X-ray diffraction data
- Trinuclear ruthenium-oxo array exhibits the trapped-valence state delocalization at room temperature
- The complex reveals to be active catalyst for hydration of nitriles and isomerization of allylic alcohols reactions.